The Astrophysical Journal, 607:90–102, 2004 May 20

POX 52: A DWARF SEYFERT 1 GALAXY WITH AN INTERMEDIATE-MASS BLACK HOLE

Aaron J. Barth,[1,2] Luis C. Ho,[3] Robert E. Rutledge,[4] and Wallace L. W. Sargent[1]

Received 2003 November 12; accepted 2004 February 3

ABSTRACT

We describe new optical images and spectra of POX 52, a dwarf galaxy with an active nucleus that was originally detected in the POX objective-prism survey. While POX 52 was originally thought to be a Seyfert 2 galaxy, the new data reveal an emission-line spectrum very similar to that of the dwarf Seyfert 1 galaxy NGC 4395, with broad components to the permitted line profiles, and we classify POX 52 as a Seyfert 1 galaxy. The host galaxy appears to be a dwarf elliptical, and its brightness profile is best fit by a Sérsic model with an index of 3.6 ± 0.2 and a total magnitude of $M_V = -17.6$. Applying mass–luminosity–line width scaling relations to estimate the black hole mass from the broad Hβ line width and nonstellar continuum luminosity, we find $M_{\rm BH} \approx 1.6 \times 10^5\ M_\odot$. The stellar velocity dispersion in the host galaxy, measured from the Ca II λ8498, 8542 lines, is 36 ± 5 km s^{-1}, also suggestive of a black hole mass of order $10^5\ M_\odot$. Further searches for active nuclei in dwarf galaxies can provide unique constraints on the demographics of black holes in the mass range below $10^6\ M_\odot$.

Subject headings: galaxies: active — galaxies: dwarf — galaxies: individual (POX 52) — galaxies: kinematics and dynamics — galaxies: nuclei — galaxies: Seyfert

1. INTRODUCTION

Studies of the dynamics of stars and gas in the nuclei of nearby galaxies have detected the signature of supermassive black holes in an ever-increasing number of galaxies (for recent reviews, see Kormendy 2004; Barth 2004), and it is now widely accepted that all galaxies with a massive bulge component contain a central black hole. While existing surveys have made great progress in the black hole census for masses in the range $\sim 2 \times 10^6 - 3 \times 10^9\ M_\odot$, very little is known about the population of black holes with masses below $10^6\ M_\odot$. Stellar-dynamical and gasdynamical searches do not have sufficient sensitivity to detect black holes of mass $\lesssim 10^6\ M_\odot$ for galaxies much beyond the Local Group. "Intermediate-mass" black holes with masses of $\sim 10^3$–$10^6\ M_\odot$ might be present in the centers of very late-type spiral galaxies, in dwarf elliptical and dwarf spheroidal galaxies, and possibly even in massive globular clusters, but thus far dynamical studies have only been carried out for a few very nearby objects, sometimes with ambiguous results (van der Marel 2004). At present, there is little hope of obtaining a systematic census of black holes with $M < 10^6\ M_\odot$ by using traditional dynamical detection techniques. The demographics of intermediate-mass black holes are of particular importance for future gravitational-wave studies, since it is expected that the most common massive black hole merger events detected by the space-based *LISA* interferometer will be in the 10^5–$10^6\ M_\odot$ range (Hughes et al. 2001).

Intermediate-mass black holes that would be undetectable by dynamical measurements might still reveal their presence by their accretion luminosity. The detection of a low-luminosity active galactic nucleus (AGN) in a dwarf galaxy would be a good indication that a black hole is present, and indirect methods could be used to estimate the black hole mass even if a stellar-dynamical mass measurement is impossible. However, only two AGNs in dwarf galaxies have been identified previously. The better known case is the nearby ($D \approx 4$ Mpc), late-type, dwarf spiral galaxy NGC 4395. Filippenko & Sargent (1989) found that NGC 4395 contains the least luminous known Seyfert 1 nucleus. Despite the fact that this galaxy has no discernible bulge, and thus might not be expected to contain a central black hole, its nucleus exhibits all of the characteristics of Seyfert activity, including broad emission lines (Filippenko & Sargent 1989), a compact, unresolved nonstellar continuum source in the optical and ultraviolet (Filippenko, Ho, & Sargent 1993), unresolved radio emission with a high brightness temperature (Wrobel, Fassnacht, & Ho 2001), and rapid X-ray variability (Iwasawa et al. 2000; Shih, Iwasawa, & Fabian 2003; Moran et al. 2004). The central stellar velocity dispersion is $\sigma_* < 30$ km s^{-1}, which, combined with the radius of the central star cluster (3.9 pc), gives a firm upper limit of $M < 6 \times 10^6\ M_\odot$ for the combined mass of the central star cluster plus black hole (Filippenko & Ho 2003). The black hole itself has a likely mass of $\sim 10^4$–$10^5\ M_\odot$, based on the X-ray variability timescale (Shih et al. 2003) and extrapolation of the line width–luminosity–mass correlations for Seyfert galaxies (Filippenko & Ho 2003). Finding more active galaxies like NGC 4395 would be a valuable step toward understanding the demographics of black holes with $M < 10^6\ M_\odot$.

POX 52 (also known as PGC 038055 or G1200−2038) is a dwarf galaxy at $cz = 6533$ km s^{-1}. It was discovered in the course of an objective-prism search for emission-line objects performed by Kunth, Sargent, & Kowal (1981). They listed the fluxes for several emission lines in POX 52 and noted that it appears "starlike" in Palomar Sky Survey images. Follow-up spectroscopy and imaging data were presented by Kunth, Sargent, & Bothun (1987, hereafter KSB). KSB called attention to POX 52 as an unusual example of a dwarf galaxy having an AGN spectrum. The object was classified as a Seyfert 2 based on the narrow-line ratios, although they noted that the Hβ line had a weak broad component with full width at half-maximum (FWHM) $\approx$840 km s^{-1}. They also found a

[1] Department of Astronomy, 105-24, California Institute of Technology, Pasadena, CA 91125.
[2] Hubble Fellow.
[3] The Observatories of the Carnegie Institution of Washington, 813 Santa Barbara Street, Pasadena, CA 91101.
[4] Theoretical Astrophysics, 130-33, California Institute of Technology, Pasadena, CA 91125.

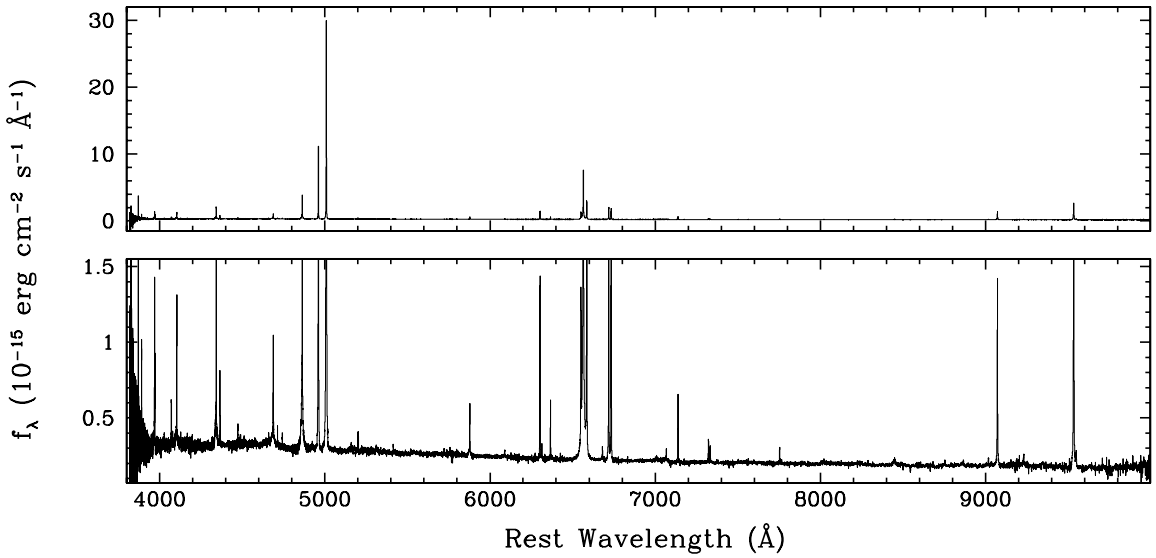

FIG. 1.—Keck ESI spectrum of POX 52

weak broad component to the He II λ4686 emission line, which they tentatively ascribed to emission from Wolf-Rayet stars. The host galaxy was found to have an exponential scale length of only 1 kpc and an absolute magnitude of $M_V = -16.9$. This is a surprisingly small host galaxy for an AGN. However, a literature search reveals that very few additional observations of POX 52 have been performed since the initial study by KSB. Motivated by the possibility that POX 52 might contain an intermediate-mass black hole similar to the one in NGC 4395, we obtained new spectra and images of POX 52 at the Keck and Las Campanas observatories.[5]

Throughout this paper we assume a Hubble constant of $H_0 = 70$ km s^{-1} Mpc^{-1}.

2. OBSERVATIONS AND REDUCTIONS

2.1. *Spectroscopy*

We observed POX 52 with the ESI spectrograph (Sheinis et al. 2002) at the Keck II telescope on the night of 2002 December 2 UT. In echellette mode, ESI gives complete coverage of the wavelength range 3800–11000 Å in 10 echelle orders, at a pixel scale of 11.5 km s^{-1} pixel^{-1}. We used a 0.″5 wide slit, for a FWHM resolution of $\sim$36 km s^{-1} as measured from the widths of arc lamp lines. The total exposure time for POX 52 was 2400 s, and the air mass ranged from 1.85 to 1.65 during the observations. The slit was oriented at P.A. = 320°, which was the parallactic angle for the midpoint of the exposure. This angle coincided almost exactly with the position angle of the host galaxy major axis, as we later determined from imaging data. On the same night, we also observed the nucleus of NGC 4395 with the same setup for 2400 s, at air mass 1.6, as well as seven giant stars of spectral type ranging from G9 III to K5 III for use as velocity dispersion templates. The seeing, in standard star exposures taken at air mass 1.2 immediately after the galaxy observations, was 0.″9–1.″0. Wavelength calibration was performed using observations of HgNe, Xe, and CuAr lamps.

The spectra were flattened, extracted, and wavelength-calibrated using both the automated MAKEE software package[6] and also using standard tasks in IRAF,[7] as a comparison. The extraction width was 2.″5. The extractions performed using the two software packages were virtually identical except for wavelengths longer than $\sim$8000 Å, where the sky subtraction was more accurate in the IRAF reductions. The extractions were then flux-calibrated and corrected for telluric absorption bands using observations of the standard star Feige 34.

2.2. *Imaging*

Optical images of POX 52 were obtained at the du Pont 2.5 m telescope at Las Campanas Observatory on the night of 2003 February 10 UT, using the Direct Tek #5 CCD Camera with a pixel scale of 0.″259. The night was photometric with $\sim$0.″75 seeing. POX 52 was observed using *B*, *V*, *R*, and *I* filters, with an exposure time of 2×360 s in each filter. Two Landolt (1992) standard star fields were observed for photometric calibration. The images were bias-subtracted and flattened, and the photometric zeropoints were determined using standard tasks in IRAF.

3. THE ACTIVE NUCLEUS

3.1. *Emission Lines*

Figure 1 displays the complete ESI spectrum of POX 52. The data confirm KSB's classification of POX 52 as a Seyfert galaxy, as demonstrated by the large [O III]/Hβ ratio and the strengths of [O I] λ6300, [N II] λ6584, and [S II] $\lambda\lambda$6716, 6731 relative to Hα.

More than 40 emission lines are visible in the spectrum. To measure the line intensities, we first fitted a low-order spline to the continuum in each echelle order and subtracted it from the spectrum. The line fluxes were measured by direct integration, or in the case of some blended lines, by performing a multi-Gaussian model fit, and the results are listed in Table 1.

[5] At the time of this writing, the SIMBAD database contains incorrect coordinates for POX 52. The correct J2000 coordinates are listed in NED as $\alpha = 12^h02^m56^s.9$, $\delta = -20°56'03''$.

[6] See http://www2.keck.hawaii.edu/inst/common/makeewww/index.html.

[7] IRAF is distributed by the National Optical Astronomy Observatories, which are operated by the Association of Universities for Research in Astronomy, Inc., under cooperative agreement with the National Science Foundation.

TABLE 1
EMISSION LINES IN POX 52

Line	Rest Wavelength (Å)	Flux (10^{-15} ergs cm^{-2} s^{-1})	$I/I(\mathrm{H}\beta_n)$
[Ne III]	3869.1	4.8	0.66
He I + Hζ	3888.6, 3889.0	1.0	0.14
[Ne III]	3967.8	1.7	0.23
Hϵ	3970.1	0.9	0.12
[S II]	4068.6	0.5	0.07
[S II]	4076.4	0.1	0.01
Hδ	4101.7	2.1	0.29
Hγ	4340.5	4.6	0.63
[O III]	4363.2	0.9	0.12
He I	4471.5	0.3	0.04
[Fe III]	4658.1	0.2	0.03
He II	4685.7	3.0	0.40
[Ar IV]	4711.4	0.2	0.03
[Ar IV]	4740.2	0.2	0.03
Hβ narrow	4861.3	7.5	1.00
Hβ broad	4861.3	3.9	0.52
[O III]	4958.9	20.9	2.78
[O III]	5006.8	60.4	8.01
[Fe VII]	5158.4	0.1	0.01
[N I]	5197.9	0.2	0.03
[N I]	5200.3	0.2	0.03
He II	5411.5	0.1	0.01
[Fe VII]	5720.7	0.1	0.01
[N II]	5754.6	0.1	0.01
He I	5875.7	1.3	0.17
[Fe VII]	6086.3	0.2	0.03
[O I]	6300.3	2.6	0.33
[S III]	6312.1	0.2	0.03
[O I]	6363.8	0.9	0.12
[N II]	6548.0	2.3	0.29
Hα narrow	6562.8	23.4	2.98
Hα broad	6562.8	11.1	1.41
[N II]	6583.5	7.2	0.92
He I	6678.2	0.4	0.05
[S II]	6716.4	5.3	0.67
[S II]	6730.8	4.7	0.60
[Ar V]	7005.4	0.1	0.01
He I	7065.3	0.3	0.04
[Ar III]	7135.8	1.3	0.16
[O II]	7318.9, 7320.0	0.5	0.06
[O II]	7329.7, 7330.7	0.4	0.05
[Ar III]	7751.1	0.3	0.04
O I	8446.4	0.6	0.07
P12	8750.5	0.3	0.04
P11	8862.8	0.2	0.02
P10	9014.9	0.2	0.02
[S III]	9068.6	4.0	0.49
P9	9229.0	0.3	0.04
[S III]	9530.6	10.0	1.22
Pϵ	9546.0	0.4	0.05
Pδ	10049.4	0.7	0.08

NOTES.—Measured line fluxes do not take into account slit losses for the observations of POX 52 or of the standard star, so the overall flux scale may be inaccurate although relative fluxes should be unaffected. Intensity ratios $I/I(\mathrm{H}\beta_n)$ are intensities relative to the narrow component of Hβ, corrected for a Galactic extinction of $A_B = 0.173$ mag, which is the mean of the extinction estimates from Burstein & Heiles 1982 and from Schlegel et al. 1998. Except for Hα and Hβ, the measured line fluxes are total fluxes for the narrow and broad components combined. The air wavelengths for emission lines are taken from the Atomic Line List at http://www.pa.uky.edu/~peter/atomic/.

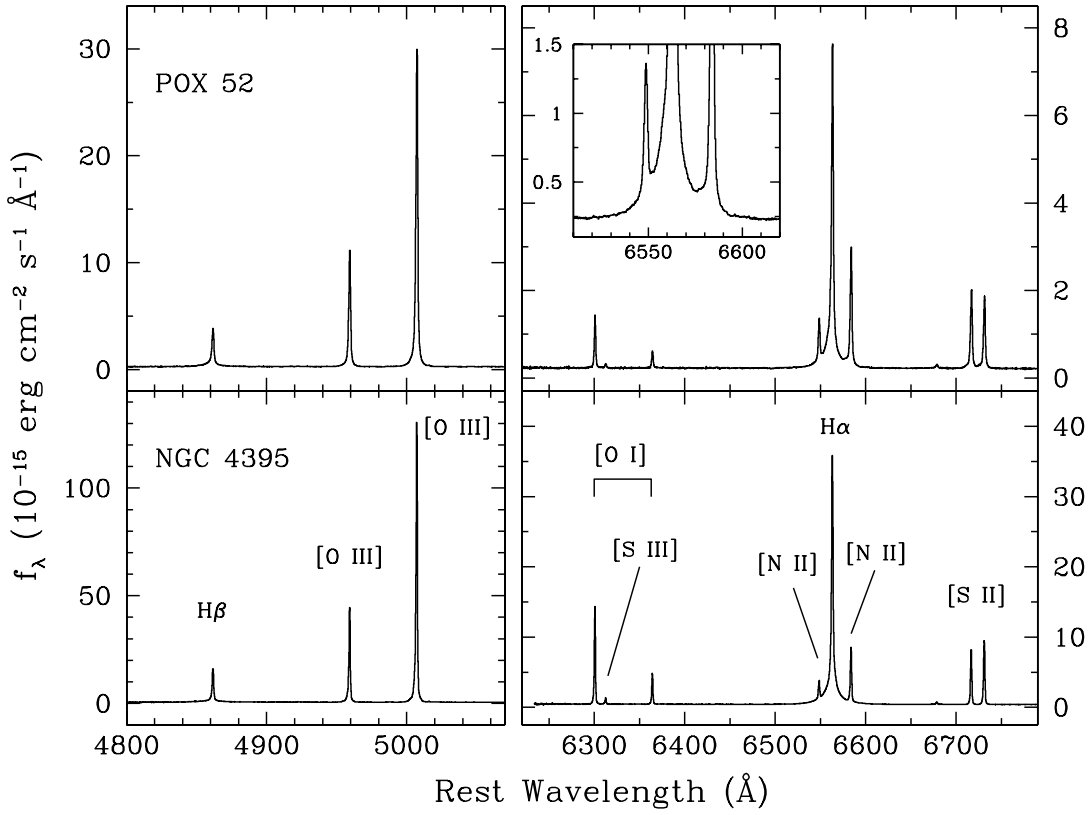

FIG. 2.—Keck ESI spectra of POX 52 and NGC 4395. For each object, the two panels show the wavelength ranges containing the Hβ and [O III] lines (*left panels*) and the [O I], Hα, [N II], and [S II] lines (*right panels*). The inset shows a close-up view of the broad base of Hα in POX 52.

Measurement uncertainties are dominated by systematics including the exact placement of the underlying continuum; we estimate that the fluxes of the strong lines are uncertain by ~5%–10%, while the uncertainties on the weakest lines may be ~40%–50%. In addition, there is an overall uncertainty to the flux scale because of slit losses, but this should not affect line ratios. The Galactic extinction toward POX 52 appears to be slightly uncertain; Burstein & Heiles (1982) give $A_B = 0.12$ mag, while Schlegel, Finkbeiner, & Davis (1998) find $A_B = 0.225$ mag along this line of sight. As a compromise, we chose to compute extinction-corrected line intensities using the mean of these two extinction values and using the reddening curve of Cardelli, Clayton, & Mathis (1989). The peak wavelengths of the 12 strongest emission lines give a heliocentric recession velocity of $cz = 6533 \pm 6$ km s^{-1}, while the stellar Mg b and Ca II triplet absorption lines yield $cz = 6531 \pm 12$ km s^{-1}. These results differ substantially from the value of 6420 km s^{-1} reported by KSB.

One notable feature of the POX 52 spectrum is the presence of [Fe VII] emission with lines at 5158, 5721, and 6086 Å. These emission lines are also found in the spectrum of NGC 4395 (Kraemer et al. 1999), and some narrow-line Seyfert 1 (NLS1) galaxies (Osterbrock & Pogge 1985). The detection of these high-excitation features further confirms the classification of POX 52 as a genuine Seyfert galaxy.

Figure 2 shows the spectral regions around [O III] and Hβ, and the region surrounding Hα, for POX 52 and NGC 4395. The two objects have extremely similar spectra, with only small differences in the line ratios and widths. POX 52 has broad wings on the Hα emission line that appear nearly identical to those in NGC 4395. KSB noted the presence of a weak broad component to the Hβ and Hα lines but still classified POX 52 as a Seyfert 2 galaxy. The broad components are clearly present in the Keck data; thus, POX 52 should be classified as a Seyfert 1 galaxy. In the Osterbrock (1981) classification scheme, POX 52 would be considered a Seyfert 1.8 galaxy; NGC 4395 falls in the same category (Ho, Filippenko, & Sargent 1997). Figure 3 displays the profiles of several permitted lines as well as [O III] λ5007 and [O I] λ6300. The broad wings are visible on the profiles of Hγ, Hβ, Hα, He II λ4686, and He I λ5876. In contrast, the [O I] and [O III] lines appear devoid of broad components.

To decompose the Hβ profile into narrow and broad components, we performed a fit to the continuum-subtracted Hβ line using a model consisting of a broad Gaussian plus a narrow component with the same profile as the [O III] λ5007 line. The free parameters in the fit included the flux and central wavelength of the narrow-line profile, and the total flux, central wavelength, and FWHM of the broad Gaussian. Figure 4 displays the best-fitting model, which has a broad-line width of FWHM(Hβ) = 760 $\pm$ 30 km s^{-1}. (We note that this is quite close to the measurement of FWHM = 840 km s^{-1} by KSB.) The need for a distinct broad component in the model fit is clearly apparent, and the broad component contains 34% of the total Hβ flux.

We performed a similar decomposition of the Hα profile, using a Gaussian for the broad component and the [O III] profile to represent the narrow Hα component and the [N II] lines. The results are more uncertain than for the Hβ model fit because of the contribution from the [N II] emission lines, and we estimate that the broad component flux for Hα listed in Table 1 may be uncertain by ~20%. However, the *total* (broad+narrow) Hα/Hβ intensity ratio (which is insensitive to the broad/narrow decomposition), corrected for Galactic

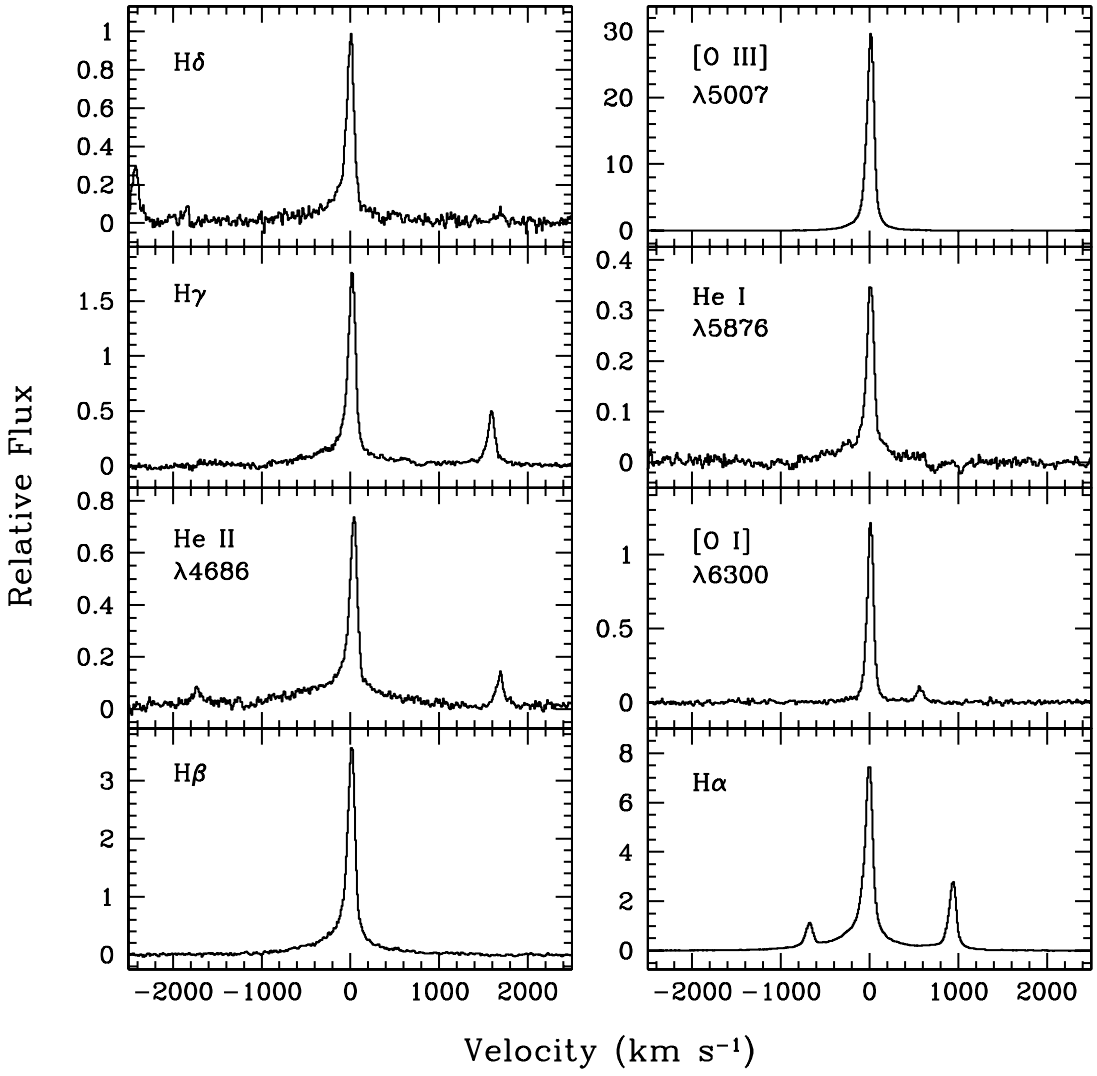

FIG. 3.—Profiles of emission lines in POX 52. The spectra have been continuum-subtracted using a low-order spline anchored to the spectra at velocities beyond ± 2000 km s^{-1} from the emission-line centers. Some residual stellar absorption features are visible.

extinction, is $I(\mathrm{H}\alpha)/I(\mathrm{H}\beta) = 2.9$, indicating that there is little internal extinction within POX 52. The width of the broad-line component is also rather uncertain because the model is a poor fit to the extended wings of Hα, but the best-fitting model has FWHM $= 765 \pm 80$ km s^{-1}, consistent with the broad Hβ line width.

Overall, the narrow-line intensities relative to Hβ are very similar to those reported by Kraemer et al. (1999) for NGC 4395. One difference, which is apparent in Figure 2, is the ratio of the [S II] $\lambda\lambda$6716, 6731 emission lines, indicating a lower density narrow-line region (NLR) in POX 52. The ratio $I(6716)/I(6731)$ is 1.12 in POX 52 and 0.88 in NGC 4395, corresponding to electron densities of $n_e \approx 360$ and 1000 cm^{-3}, respectively, for $T_e = 10^4$ K. The lower [O I]/[S II] ratio is also indicative of a lower density NLR in POX 52. The larger [N II]/Hα ratio in POX 52 suggests that it may have a higher nitrogen abundance than NGC 4395; Kraemer et al. (1999) have shown that the NGC 4395 nucleus has a low N/O ratio of about 1/3 solar.

KSB found that the widths of the narrow lines in POX 52 were marginally resolved in comparison with their arc lamp spectrum, and inferred an intrinsic line width of FWHM $=$ 320 km s^{-1} for the narrow emission lines in POX 52. The ESI data show that the forbidden lines are much narrower than this estimate as previously noted by Whittle (1992). The [O III] λ5007 line width was measured in three different ways: by a direct measurement of the full width at half of the peak flux (FWHM $= 93$ km s^{-1}), by a Gaussian fit (FWHM $= 102$ km s^{-1}), and by a Lorentzian fit (FWHM $= 83$ km s^{-1}). Neither model fit proved to fit the asymmetric line profile particularly well, and we adopt FWHM $= 93 \pm 10$ km s^{-1} as the best estimate of the observed line width. Subtracting the instrumental FWHM of 0.56 Å (measured from arc lamp exposures) in quadrature, the intrinsic line width is then FWHM([O III]) $=$ 87 ± 10 km s^{-1}.

3.2. *X-Ray and Radio Data*

As a Seyfert 1 galaxy, POX 52 should contain a central X-ray source. We searched the available X-ray archives[8] for images containing the position of POX 52 and found only one matching data set, from the *ROSAT* all-sky survey (Voges et al. 1999). This survey scanned the sky with the *ROSAT* PSPC detector (0.4–2.4 keV energy band), covering each point on average with a $\sim$300 s integration. The typical 1 σ positional

[8] See http://heasarc.gsfc.nasa.gov.

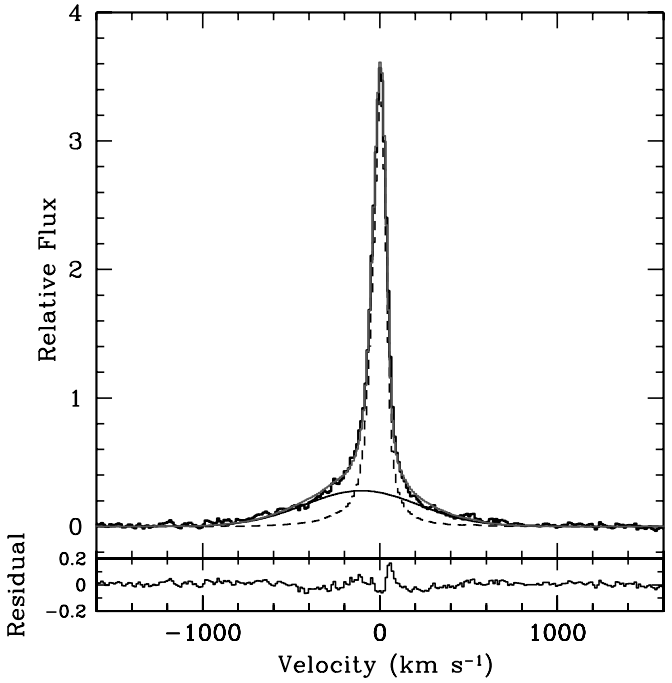

FIG. 4.—Model fit to the Hβ line, including a scaled version of the [O III] λ5007 profile (*dashed line*) for the narrow component and a Gaussian for the broad component. The residuals of the best-fitting model are shown in the lower panel.

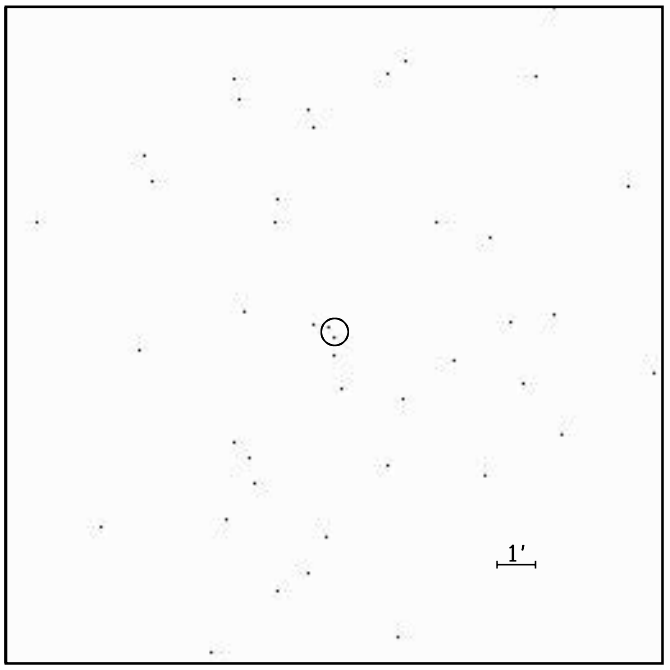

FIG. 5.—Portion of the *ROSAT* All-Sky Survey image of the field surrounding POX 52. Each point corresponds to one X-ray count. The error circle is centered on the position of POX 52 and has $r = 21''$. North is up, and east is to the left.

uncertainty is $12''$, which includes a systematic uncertainty of $6''$, largely due to boresight corrections. The FWHM of the PSPC point-spread function (PSF) is $20''$. The exposure time for the field surrounding POX 52 was only 90 ± 2 s, where the uncertainty is the range of exposure in adjacent $15''$ cells.

There is no obvious, strong X-ray source at the position of POX 52, but careful examination of the image does reveal a localized excess above the background count rate. The 75% energy radius (that is, the radius that would enclose 75% of the PSPC PSF) is $20''$ (Boese 2000). Combining the $20''$ radius for the PSF with the $6''$ systematic uncertainty (summed in quadrature), we took a region of radius $21''$ about the known position of POX 52 in the *ROSAT* data and found two counts within it (see Fig. 5). In the surrounding $1800''$ radius region, there were 370 counts, giving a mean background level of $\rho = 3.6 \times 10^{-5}$ counts per square arcsecond. Then, the probability of two background events falling within an error circle with $r = 21''$ is $P_2(r = 21'') = [1 - \exp(-\rho\pi r^2)]^2 = 0.2\%$. If we permit the error circle to expand to $r = 30''$ (at which point there is a third count) the probability of chance coincidence of two counts at this location can be as high as 0.9%.

Examination of the properties of the two counts showed them to be of low energy, occurring in pulse-height invariant (PI) channels 57 and 58, at approximately 0.5 keV. Taking only PI channels 20–80 for background, this decreases the background rate to 1.7×10^{-5} counts per square arcsecond. Subsequently, the significance for two counts within $21''$ becomes 0.04%, and within $30''$ is 0.2%. We adopt the significance of detection to be in the range of 0.04%–0.2% (3.0–3.5 σ).

The observed energy fluence from this source is approximately 1 keV. Using Poisson statistics to determine the counting uncertainty (Gehrels 1986), the detection contains $2^{+2.6}_{-1.9}$ counts (1 σ Poisson error bars). The detector area at 0.5 keV is $\sim$500 cm^2, and total flux from the source is $(4.0^{+5.2}_{-3.8}) \times 10^{-14}$ ergs cm^{-2} s^{-1}. For $D = 93$ Mpc, this corresponds to a time-averaged luminosity of $(4.3^{+5.6}_{-4.1}) \times 10^{40}$ ergs s^{-1}. Note that the detection certainty is higher than indicated by the flux uncertainty.

Unfortunately, given the shallowness of the *ROSAT* exposure and the bare 3.0–3.5 σ significance of the source detection, the best that can be done is to extract a very rough estimate of the X-ray luminosity. It would be extremely worthwhile to observe POX 52 with *Chandra* or *XMM-Newton* to confirm this detection and to properly quantify its X-ray luminosity, spectral shape, and variability, particularly in light of the extreme short-timescale variability recently found in NGC 4395 (Shih et al. 2003; Moran et al. 2004).

A *ROSAT* observation of NGC 4395 by Moran et al. (1999) revealed a soft X-ray luminosity of 3.4×10^{38} ergs s^{-1} (after rescaling to $D = 4.2$ Mpc). Taking our *ROSAT* measurement at face value, POX 52 is then $\sim$100 times more luminous than NGC 4395 in soft X-rays, although this is at best a rough comparison because of the large uncertainty in the *ROSAT* measurement as well as the possibility of strong X-ray variability in POX 52.

We searched for POX 52 in the NRAO VLA Sky Survey archives (Condon et al. 1998) and did not find a source at the galaxy's position. This implies a 3 σ upper limit of $\sim$1.4 mJy at 1.4 GHz. The field of POX 52 was not observed in the VLA FIRST survey.

4. THE HOST GALAXY

4.1. *Stellar Velocity Dispersion*

Numerous stellar absorption features are visible in the ESI spectrum, making it possible to measure the stellar velocity dispersion σ_*. We determined σ_* from the Ca II near-infrared triplet lines, which are generally the best features for measurement of stellar kinematics (Dressler 1984), and also from the region surrounding Mg b.

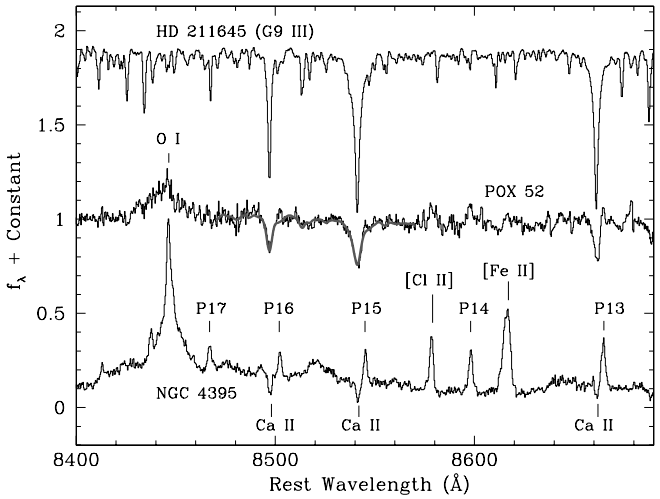

FIG. 6.—Ca II triplet spectral region in POX 52, NGC 4395, and the G9 III star HD 211645. All spectra have been rescaled to a median flux level of unity, and the spectra of HD 211645 and NGC 4395 were then shifted vertically for clarity. The smooth curve overplotted on the spectrum of POX 52 is the stellar spectrum after broadening and dilution by the featureless continuum. The identification of [Cl II] λ8578.7 in NGC 4395 is supported by the additional detection of [Cl II] λ9123.6 in the same spectrum. [Cl II] λ8578.7 emission appears to be very weakly present in POX 52 as well. This line has previously been detected in NGC 4151 (Osterbrock et al. 1990) and NGC 1068 (Osterbrock & Fulbright 1996).

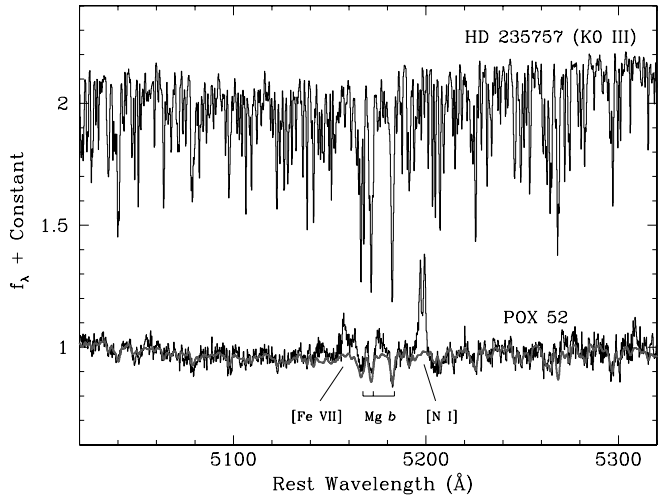

FIG. 7.—Spectral region surrounding the Mg *b* lines in POX 52 and in the K0 III star HD 235757. Both spectra were rescaled to a median flux level of unity, and the spectrum of HD 235757 was then shifted vertically by 1.0 units for clarity. The smooth curve overplotted on the spectrum of POX 52 is the stellar template after broadening and dilution by the featureless continuum. The region 5140–5210 Å was excluded from the calculation of χ^2 in the model fitting, because of the presence of emission lines.

Filippenko & Ho (2003) have recently published high-resolution spectra of the Ca triplet spectral region for NGC 4395 and determined an upper limit to its stellar velocity dispersion ($\sigma_* < 30$ km s^{-1}). The spectrum of NGC 4395 presented particular problems for this measurement, because the Ca II λ8542 and λ8662 absorption features were almost completely filled in by the Paschen-series P16 and P15 emission lines. This left Ca II λ8498 as the only uncontaminated stellar feature that could be used to measure σ_*. The P16 emission line is located 6 Å redward of Ca II λ8498, but in NGC 4395 the emission and absorption lines are sufficiently narrow that the two features do not overlap. The presence of higher order Paschen emission lines is an unusual characteristic of NGC 4395 and POX 52, which have extremely narrow emission lines of relatively high equivalent width. In most Seyfert galaxies the high-order P13–P17 lines are not visible at all; it is much more common to see the Ca II lines themselves in emission, particularly in NLS1 galaxies having strong Fe II emission (e.g., Persson 1988).

In POX 52, some high-order Paschen-series emission lines are visible (Table 1) but their equivalent widths are smaller than those in NGC 4395, as shown in Figure 6. The Ca II λ8662 line is partly filled in by P13 emission, but the 8498 and 8542 Å absorption lines appear to be largely uncontaminated, and we use those lines to determine σ_*.

The measurement was performed by a direct fit of Gaussian-broadened stellar spectra to the POX 52 spectrum over the range 8470–8570 Å, following the techniques described by Barth, Ho, & Sargent (2002). The model-fitting code broadens the stellar template by convolution with a Gaussian in velocity space and allows an additive featureless continuum contribution and a multiplicative correction described by a low-order polynomial (a quadratic in this case) to account for reddening or other differences in overall spectral shape between the galaxy and the template star. The fit of the broadened template star to the galaxy spectrum is performed directly in pixel space so that individual spectral features such as emission lines can be masked out from the computation of χ^2. The result for POX 52 is $\sigma_* = 36 \pm 5$ km s^{-1}, where the uncertainty is the sum in quadrature of the fitting error for the best-fitting template star (HD 211645, G9 III) and the standard deviation of the velocity dispersions measured from all seven template stars. The model fits include a featureless continuum that contributes ~60%–65% of the total flux in the extracted spectrum at 8500 Å to match the dilution of the stellar features. One concern is that weak Paschen emission could be partly filling in the red wings of the Ca II 8498 and 8542 Å absorption lines, which would make the above result an underestimate of the true velocity dispersion. To test this possibility, we performed the measurement again, fitting only to the core and blue wing of each absorption line, and the surrounding continuum, but excluding the red wing of both Ca lines from the fit (i.e., the regions that would be most strongly affected by Paschen emission). The best-fitting template star then gave $\sigma_* = 39 \pm 7$ km s^{-1}, in agreement with the 1 σ uncertainty range of our original measurement. Thus, the result $\sigma_* = 36 \pm 5$ km s^{-1} appears to be robust even if there is slight contamination by the P15 and P16 emission lines.

As an additional check on this result, we also performed model fits to the spectral region surrounding the Mg *b* absorption lines. As shown in Figure 7, the Mg *b* lines are contaminated by emission from [Fe VII] λ5158 and from [N I] $\lambda\lambda$5198, 5200, as well as a broad "bump" in the spectrum over ~5160–5180 Å, which may be a blend of weaker emission lines. Therefore, we fit broadened stellar templates to the regions immediately surrounding Mg *b*, from 5020 to 5320 Å but excluding the region 5140–5210 Å from the χ^2 minimization. The result, $\sigma_* = 38 \pm 4$ km s^{-1}, is consistent with the dispersion measured from the Ca II lines, and the broadened template gives a reasonable fit to the galaxy spectrum except at wavelengths affected by the emission lines.

4.2. *Photometric Decomposition*

KSB found that the luminosity profile of POX 52 was best represented by an exponential disk model with a central point

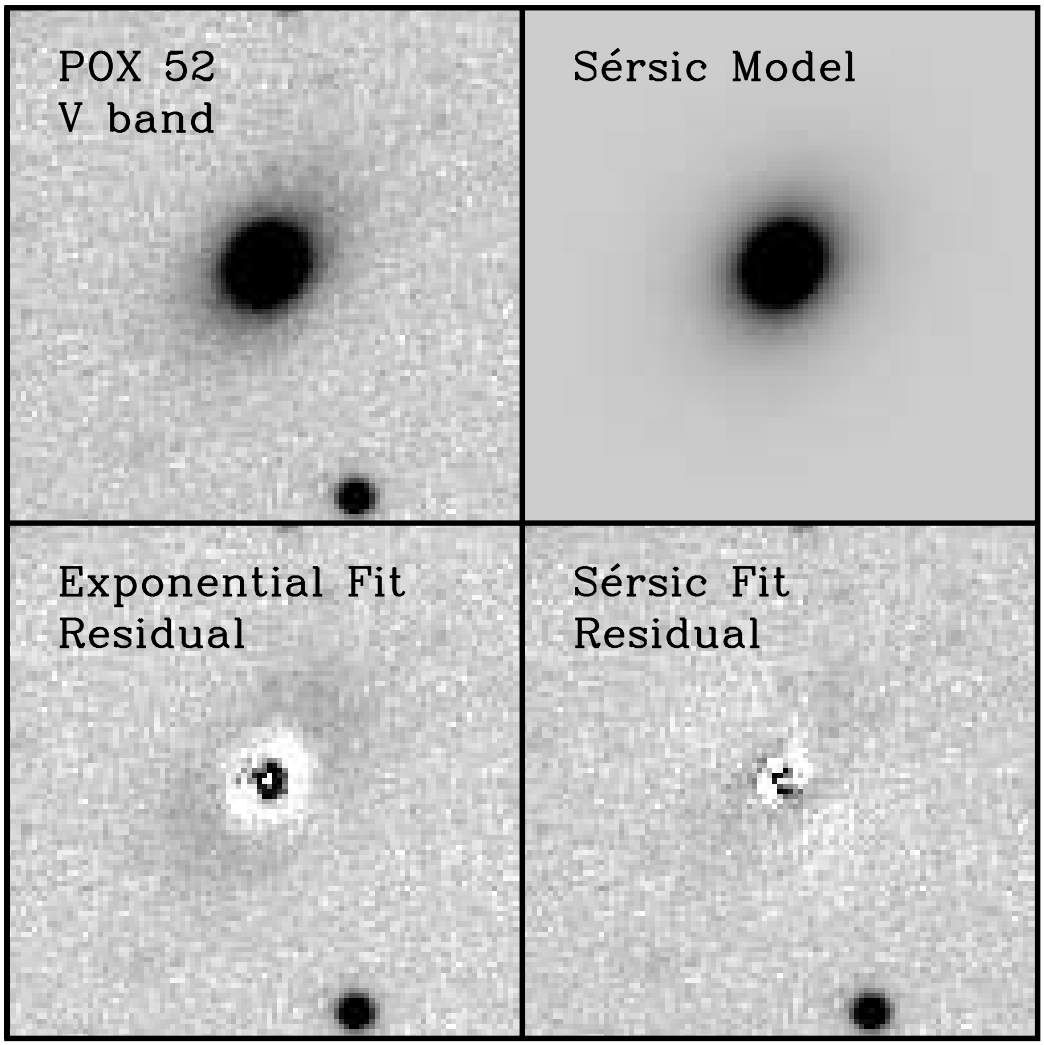

FIG. 8.—*V*-band image of POX 52. The image size is 25″ on a side. The four panels show the original data, the best-fitting Sérsic model for the host galaxy, the residual from the best fitting exponential+point source model, and the residual from the best-fitting Sérsic+point source model. Each image is displayed with the same logarithmic color stretch. The images are oriented so that north is up, and east is to the left.

source, and we expected that our optical imaging data would show spiral structure or evidence for recent star formation in a host galaxy similar to NGC 4395. However, the new images reveal a very different morphology for POX 52. There is no obvious spiral or disklike structure in the images, and none of the images shows any obvious clumpiness such as might be expected from star-forming regions in the host galaxy. As shown in Figure 8, the optical structure of POX 52 is most suggestive of a small elliptical galaxy with a bright nuclear point source.

To study the structure of the host galaxy quantitatively, we fit models to the galaxy's luminosity profile using the two-dimensional fitting code GALFIT (Peng et al. 2002). GALFIT is designed to optimize model fits to galaxy images, allowing multicomponent models with bulge, disk, and point-source components, and including convolution of the model by the telescope point-spread function. The PSF for each filter was determined from about 10 unsaturated stars in each image, using standard routines in IRAF. However, the nucleus of POX 52 was brighter than any of the unsaturated stars in the image, and the resulting PSF models proved to be somewhat noisy. We created noise-free model PSFs by fitting a two-dimensional Moffat function to the empirical PSF for each filter, and the model PSFs were then used in the GALFIT fitting.

The fitting was performed for each filter using two different galaxy models: an exponential profile plus central point source, and a Sérsic $r^{1/n}$ profile (Sérsic 1968) with index n allowed to vary, plus central point source. For each model fit, the free parameters included the host galaxy scale length or effective radius r_e, magnitude, centroid, major axis position angle, and ellipticity, and the point source magnitude and centroid. A boxiness/diskiness parameter for the host galaxy was also allowed to vary. Figure 8 shows the fitting results for the V band; we found similar results for the other bands. In each case, we found that the exponential profile was an extremely poor model for the host galaxy structure, and the best-fitting exponential profile plus point source model left a characteristic residual pattern of concentric positive and negative "rings."

While the exponential disk models were clearly inadequate, the Sérsic model fits were much more successful. The Sérsic fits still left substantial residuals within the inner $r \approx 1''$, but the residuals appeared to be more random, and confined to smaller radii, than the systematic residuals of the exponential fits. After subtracting the best-fitting Sérsic model, there is no

TABLE 2
RESULTS FROM GALAXY PROFILE FITS

	Point Source		Host Galaxy			
Band	$m_{\rm point}$	$M_{\rm point}$	$m_{\rm host}$	$M_{\rm host}$	Sérsic n	r_e (arcsec)
B	18.3	−16.7	18.3	−16.8	3.9	1.2
V	17.9	−17.1	17.4	−17.6	3.5	1.2
R	17.6	−17.4	16.7	−18.2	3.7	1.2
I	17.4	−17.5	16.3	−18.6	3.4	1.5

NOTES.—Apparent magnitudes (m) are not corrected for extinction. Absolute magnitudes (M) are corrected for extinction of $A_B = 0.173$ mag and computed for $D = 93$ Mpc.

indication of any residual spiral structure in the host galaxy. The magnitudes of the point source and host galaxy, and the Sérsic indices and effective radii, from the best-fitting models are given in Table 2. Combining the measurements from all four bands, the model fits give a Sérsic index of $n = 3.6 \pm 0.2$, close to a de Vaucouleurs law (de Vaucouleurs 1948), which corresponds to $n = 4$, and $r_e = 590 \pm 50$ pc. The model fits also gave the following results (averaged over all four bands): major axis P.A. $= 45^\circ \pm 6^\circ$, axis ratio $b/a = 0.79 \pm 0.03$, and boxiness/diskiness parameter =0.07 ± 0.10 (with positive numbers representing boxy isophotes). Figure 9 shows the radial profiles of the galaxy and the exponential and Sérsic models for the V band; the one-dimensional profiles show that the Sérsic model is a better fit than the exponential model for $r \gtrsim 1''$.

The uncertainties in the derived magnitudes are dominated by systematic errors in the fits, mainly because of the PSF models and the possible systematic deviation of the host galaxy from a pure Sérsic profile. We estimate these uncertainties to be of order ∼0.2 mag for the point source and host galaxy magnitudes listed in Table 2.

The dereddened AGN point source colors are consistent with a power-law slope in the range $\alpha \sim 1$–1.5 for $f_\lambda \propto \lambda^{-\alpha}$, although a single power-law model cannot simultaneously fit the *BVRI* measurements.

5. DISCUSSION

5.1. *Black Hole Mass*

The mass of the black hole in POX 52 can only be estimated using indirect techniques. For Seyfert 1 galaxies and quasars, there is a well-established correlation between the broad-line region radius ($r_{\rm BLR}$) and the nonstellar continuum luminosity in the optical, which has been calibrated by reverberation mapping measurements of the time delay between continuum and broad-line flux variations (Kaspi et al. 2000). If the BLR gas kinematics are dominated by gravitational motion (rather than by winds or outflows or other motions), then the broad-line widths can be combined with the BLR radius to give a virial estimate of $M_{\rm BH}$. We use the calibration of the BLR size-luminosity relationship from Kaspi et al. (2000):

$$r_{\rm BLR} = (32.9 \pm 2.0)\left[\frac{\lambda L_\lambda(5100\ \text{Å})}{10^{44}\ \text{ergs s}^{-1}}\right]^{(0.700\pm0.033)} \text{lt-days}, \quad (1)$$

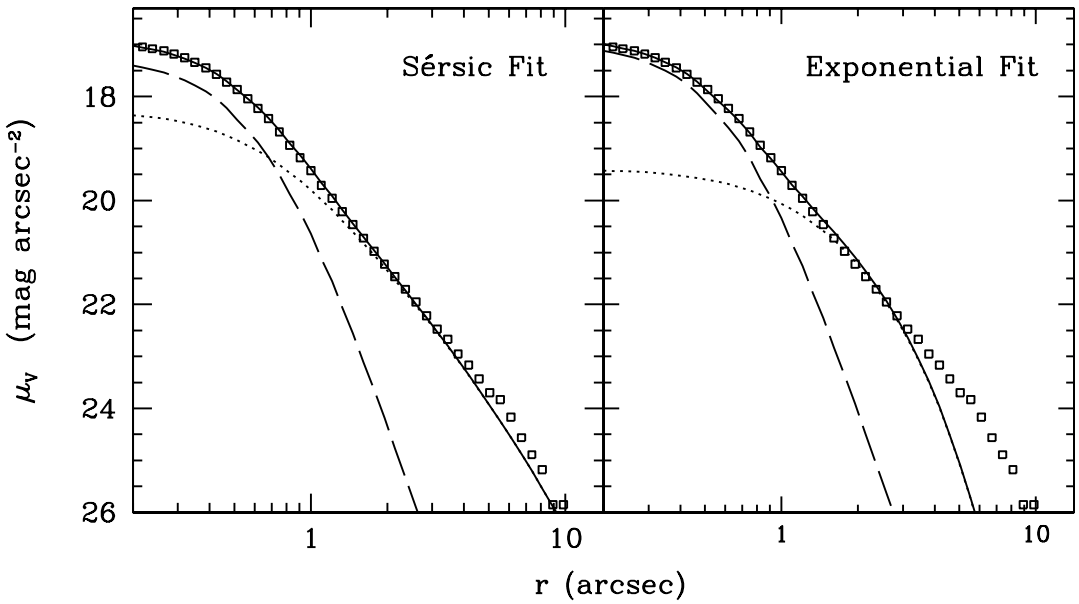

FIG. 9.—*V*-band radial profile of POX 52, compared with a Sérsic model fit (*left panel*) and an exponential profile fit (*right panel*). In each panel, the dashed curve is the point-source component, the dotted curve is the host galaxy model, and the sold curve is the combined point source+host galaxy model. The point-source and host galaxy radial profiles were measured from the two-dimensional output files produced by GALFIT using the IRAF "ellipse" task.

where $L_\lambda(5100\ \text{Å})$ is the luminosity of the nonstellar continuum at 5100 Å. The central mass is then derived from $r_{\rm BLR}$ and the Hβ line width according to

$$M_{\rm BH} = 1.5 \times 10^5 \left(\frac{r_{\rm BLR}}{\text{lt-days}}\right)\left(\frac{v_{\rm FWHM}}{10^3\ \text{km s}^{-1}}\right)^2 M_\odot, \quad (2)$$

where $v_{\rm FWHM}$ is the FWHM, in velocity units, of the broad component of Hβ. The calibration of the size-luminosity relationship is subject to some uncertainty, as discussed in detail by Vestergaard (2002), as its slope for Seyfert galaxies is somewhat different from that for quasars, and also dependent on whether or not the discrepant galaxy NGC 4051 is included in the fitting. Another issue is how $v_{\rm FWHM}$ is to be measured. Kaspi et al. (2000) measured FWHM(Hβ) in the rms spectrum from an entire reverberation campaign, which isolates the variable portion of the emission line. For POX 52 we have only a single-epoch measurement. As shown by Vestergaard (2002), single-epoch measurements of $v_{\rm FWHM}$ for a given AGN tend to cluster around the value of FWHM(Hβ, rms) with roughly $\sim$20%–25% scatter, so the use of a single-epoch FWHM should be a reasonable approximation to the rms line width.

Vestergaard (2002) has argued that single-epoch measurements of $v_{\rm FWHM}$ for quasars should be performed on the total Hβ profile, including any narrow component that might be present. However, POX 52 and NGC 4395 are extreme cases in the sense of having very weak broad components with strong narrow components that dominate the total Hβ flux. For these objects, the FWHM of the *total* Hβ profile is roughly an order of magnitude smaller than that of the broad component alone, so the width of the full Hβ profile would have almost no sensitivity to the broad component. In the Seyferts and quasars used to determine the line width-luminosity correlation, Hβ is dominated by the broad component, sometimes containing a weak bump of narrow-line emission. For an appropriate comparison between POX 52 and the calibration sample, the best option is to use only the broad-line component to determine $v_{\rm FWHM}$ and hence $M_{\rm BH}$, following the approach used by Filippenko & Ho (2003) for NGC 4395.

From the GALFIT decomposition, the extinction-corrected *B*-band absolute magnitude for the point source component is $M_B = -16.7$ mag, corresponding to $\lambda L_\lambda(5100\ \text{Å}) = 1.6 \times 10^{42}$ ergs s^{-1}. Then, for $v_{\rm FWHM} = 760$ km s^{-1}, equations (1) and (2) yield $r_{\rm BLR} \approx 1.8$ lt-days and $M_{\rm BH} \approx 1.6 \times 10^5\ M_\odot$. This mass estimate is admittedly quite uncertain. The line width–mass–luminosity relations have only been calibrated for masses greater than $10^6\ M_\odot$ (Kaspi et al. 2000), so an order-of-magnitude extrapolation is required if this method is to be applied to POX 52. In addition, there appears to be significant intrinsic scatter in these relations, and the Hβ method may yield masses that are uncertain by a factor of $\sim$3 (e.g., Peterson 2003). A further caveat is that the imaging and spectroscopic observations were not simultaneous, and the active nucleus in POX 52 could be variable on short timescales. Nevertheless, even bearing these uncertainties in mind, the resulting mass estimate indicates that the black hole in POX 52 most likely has a mass well below $10^6\ M_\odot$.

With this estimate, it is possible to examine whether POX 52 follows the correlations between black hole mass and host galaxy properties. For the $M_{\rm BH}$-σ_* relation, we use the recent fit by Tremaine et al. (2002):

$$\log(M_{\rm BH}/M_\odot) = \alpha + \beta \log(\sigma_*/200\ \text{km s}^{-1}), \quad (3)$$

where $\alpha = 8.13 \pm 0.06$ and $\beta = 4.02 \pm 0.32$. The galaxies used to calibrate this relation have σ_* ranging from 67 to 385 km s^{-1}. Extrapolating this correlation to 36 ± 5 km s^{-1}, the expected black hole mass is $(1.4 \pm 1.1) \times 10^5\ M_\odot$, where the uncertainty includes both the measurement error on σ_* for POX 52 and the uncertainty in the fitted parameters of the $M_{\rm BH}$-σ_* relation. The agreement between the black hole mass estimated from FWHM(Hβ) and the mass expected from the $M_{\rm BH}$-σ_* relation is surprisingly good, given the substantial uncertainties in both estimates. With two independent methods both suggesting a black hole mass of order $10^5\ M_\odot$, POX 52 becomes the second example (after NGC 4395) of a "dwarf" AGN with an intermediate-mass black hole.

The correlation between black hole mass and host galaxy bulge luminosity ($L_{\rm bul}$) can also be compared with this $M_{\rm BH}$ estimate, since the photometric decomposition suggests that the host galaxy light is predominantly from a bulge or spheroidal component with little or no disk contribution. Using the fit to the $M_{\rm BH}$-$L_{\rm bul}$ correlations from Kormendy & Gebhardt (2001) and from Marconi & Hunt (2003), which use *B*-band bulge luminosities, the implied value of $M_{\rm BH}$ is in the range $(5.0-7.3) \times 10^6\ M_\odot$. This is more than an order of magnitude larger than the mass derived from the Hβ line width, and it is an extreme case in terms of the large disagreement between the $M_{\rm BH}$-σ_* relation and the $M_{\rm BH}$-$L_{\rm bul}$ relation. The $M_{\rm BH}$-σ_* correlation is generally thought to have smaller scatter than the $M_{\rm BH}$-$L_{\rm bul}$ correlation (Ferrarese & Merritt 2000; Gebhardt et al. 2000), although Marconi & Hunt (2003) claim that $M_{\rm BH}$ correlates most tightly with bulge mass rather than with σ_* or luminosity alone. There appears to be an extremely large amount of scatter in the *B*-band $M_{\rm BH}$-$L_{\rm bul}$ relation for $M_{\rm B,bul} > -18$ mag; as Kormendy & Gebhardt (2001) point out, the total range in $M_{\rm BH}$ is 2 orders of magnitude for a given value of $L_{\rm bul}$. All of the galaxies currently used to calibrate the $M_{\rm BH}$-σ_* correlation have $\sigma_* \geq 67$ km s^{-1} and $M_{\rm BH} > 2 \times 10^6\ M_\odot$, so there are no galaxies with known $M_{\rm BH}$ that are comparable in overall properties to POX 52. The best hope for a local calibrator in this mass range may be the Local Group dwarf elliptical galaxy NGC 205, which has a central velocity dispersion of 30 km s^{-1} (Bender, Paquet, & Nieto 1991) and $M_B = -15.4$ mag and is close enough that a measurement of $M_{\rm BH}$ with the *Hubble Space Telescope* should be feasible.

To determine the Eddington ratio $L/L_{\rm Edd}$, we estimate the bolometric luminosity ($L_{\rm bol}$) of the AGN, using the optical continuum luminosity combined with a bolometric correction based on either the spectral energy distribution (SED) of NGC 4395, or that of a normal quasar. If we assume that POX 52 has an SED similar to that of NGC 4395, then the ratio of the bolometric luminosities of the two objects will be similar to the ratio of optical AGN luminosities. Following Filippenko & Ho (2003), we assume a distance of 4.2 Mpc to NGC 4395. Using either the *B*-band continuum flux of the NGC 4395 nucleus (Filippenko & Sargent 1989) or its narrow Hβ flux (Kraemer et al. 1999), we find that the AGN in POX 52 is approximately 200 times more luminous than the one in NGC 4395. NGC 4395 has a bolometric luminosity of $\sim 5 \times 10^{40}$ ergs s^{-1} (Moran et al. 1999, rescaled to $D = 4.2$ Mpc); this implies $L_{\rm bol} \approx 1 \times 10^{43}$ ergs s^{-1} for POX 52. Alternatively, applying the standard quasar *B*-band bolometric correction from Elvis et al. (1994), the estimated bolometric luminosity is 2×10^{43} ergs s^{-1}. Then, for $M_{\rm BH} = 1.6 \times 10^5\ M_\odot$, the Eddington ratio is in the range $L_{\rm bol}/L_{\rm Edd} \approx 0.5-1$. Thus, the black hole in POX 52 appears to be radiating at nearly its maximal rate, and it may be undergoing a major

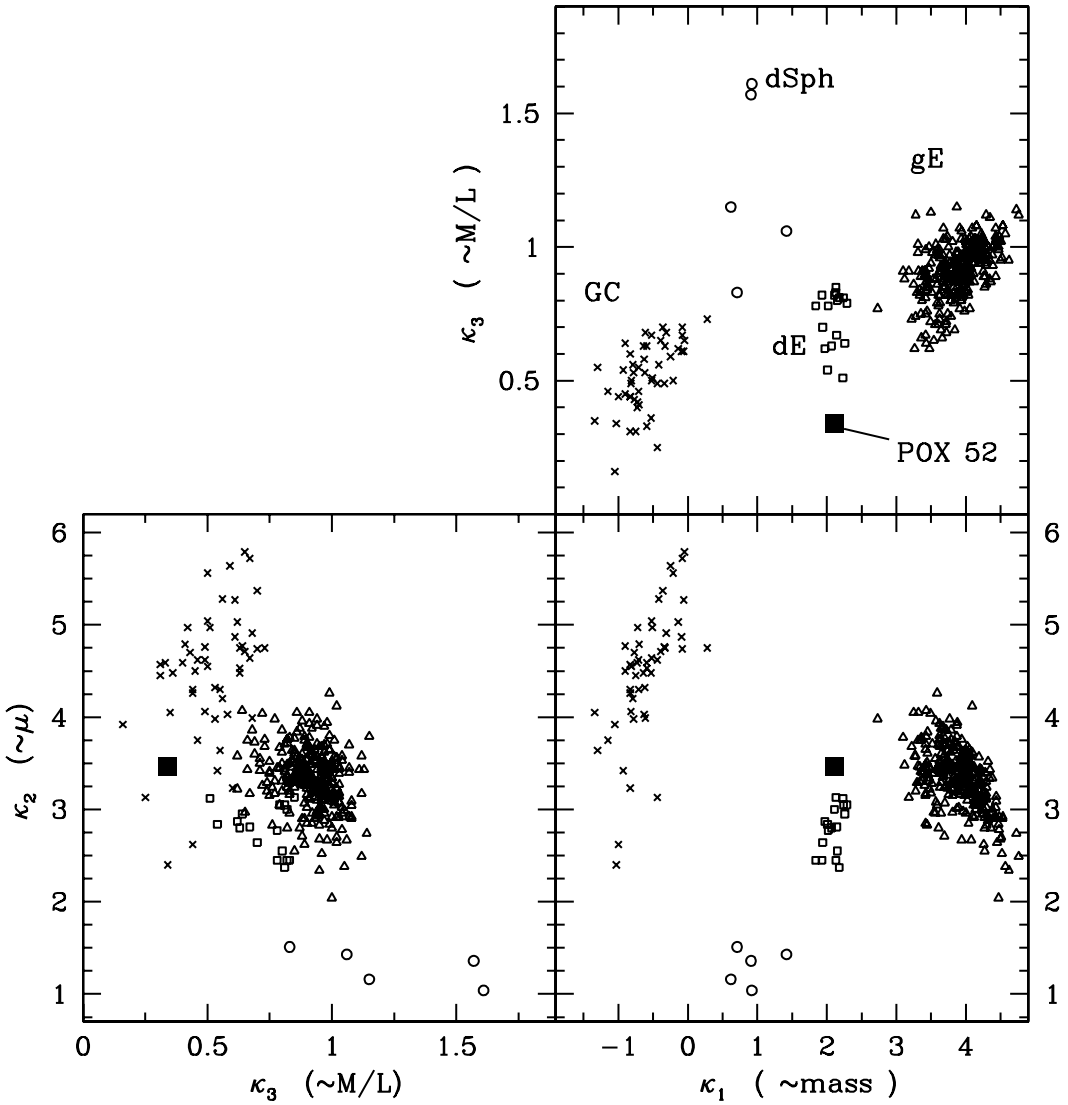

FIG. 10.—"κ-space" projections of the fundamental plane, following Burstein et al. (1997) and Geha et al. (2003). The parameters κ_1, κ_2, and κ_3 are related to galaxy mass, surface brightness, and mass-to-light ratio. Data points taken from Burstein et al. (1997) include giant elliptical galaxies (*triangles*), dwarf spheroidals (*circles*), and globular clusters (*crosses*). Dwarf elliptical galaxies (*open squares*) are from Geha et al. (2003). POX 52 is shown as a large filled square.

episode of mass accretion. In contrast, Filippenko & Ho (2003) estimated $L_{\rm bol}/L_{\rm Edd} \approx 2 \times 10^{-2}$–$2 \times 10^{-3}$ for NGC 4395. Given the apparently large difference in the accretion rates of these two objects, the overall similarity in their optical spectra is somewhat surprising.

Assuming that $L_{\rm bol} \leq L_{\rm Edd}$ in POX 52, a lower limit to $M_{\rm BH}$ can be derived. The smaller estimate of $L_{\rm bol}$ (1×10^{43} ergs s^{-1}) implies $M_{\rm BH} \geq 7 \times 10^4\ M_\odot$.

5.2. *Host Galaxy and Environment*

What type of galaxy is POX 52? The GALFIT profile measurements indicate that it is unlikely to be a pure disk galaxy. Its absolute magnitude and effective radius are within the normal range for dwarf ellipticals, and its ($B-V$) color of 0.8 mag is also typical of dwarf ellipticals (Gavazzi et al. 2001). However, the Sérsic index of 3.6 ± 0.2 is outside the usual range of ~1.0–3.0 for dwarf ellipticals in Virgo (Geha, Guhathakurta, & van der Marel 2003).

To examine whether POX 52 is closer in properties to dwarf or giant ellipticals, it is useful to determine its location in the fundamental plane. We use the "κ-space" projections of the fundamental plane, as defined by Bender, Burstein, & Faber (1992) and Burstein et al. (1997). In this projection, the fundamental plane is viewed along axes that correspond to galaxy mass (κ_1), surface brightness (κ_2), and mass-to-light ratio (κ_3). Dwarf ellipticals, giant ellipticals, dwarf spheroidals, and globular clusters are well-segregated in κ-space, as shown by Burstein et al. (1997) and Geha et al. (2003). Combining our B-band host galaxy parameters with the stellar velocity dispersion, we find $\kappa_1 = 2.11$, $\kappa_2 = 3.47$, and $\kappa_3 = 0.34$ for POX 52. Figure 10 illustrates the position of POX 52 in the κ-space projections, in comparison with data from the literature. POX 52 lies closest to the family of dwarf ellipticals, although it is slightly offset from the Virgo dwarf ellipticals studied by Geha et al. (2003) in the sense of having somewhat higher surface brightness and lower mass-to-light ratio. One possible explanation could be a younger stellar population in POX 52 than in the Virgo dwarf ellipticals, but this may be unlikely given the normal ($B-V$) color of POX 52. A more likely explanation may be systematic uncertainty in the GALFIT decomposition; the unusual Sérsic index for POX 52 could be the result of an imperfect model fit to the

host galaxy resulting from the presence of the extremely bright central point source. Imaging data from the *Hubble Space Telescope* would provide a much more accurate decomposition into point-source and host galaxy components and a better measurement of the Sérsic index and the galaxy profile within the inner arcsecond. With the present data, we conclude that POX 52 is best classified as a dwarf elliptical, although perhaps a peculiar one.

To our knowledge, no other dwarf elliptical galaxy has been found to host a Seyfert nucleus. One object that has been referred to as a dwarf elliptical with an AGN is the nearby galaxy NGC 3226 (George et al. 2001). Its nucleus is a LINER with a broad component to the Hα emission line (Ho et al. 1997), and it is also an X-ray source (George et al. 2001). While there is no question that NGC 3226 hosts a genuine AGN, it is too massive and too large to be classified as a true dwarf elliptical galaxy. It has an absolute magnitude of $M_B = -19.4$ and $\sigma_* \approx 180$ km s^{-1} (Simien & Prugniel 1998), which suggests a likely black hole mass of order $10^8\ M_\odot$ from the $M_{\rm BH}$-σ_* relation. Thus, NGC 3226 appears to be a small but ordinary elliptical, probably with a fairly massive black hole that is accreting at an extremely sub-Eddington rate, and it is very different from the "dwarf AGNs" in POX 52 and NGC 4395 with $M_{\rm BH} < 10^6\ M_\odot$.

Nelson & Whittle (1996) found a correlation between the stellar and gaseous line widths in Seyfert galaxies. The near equality between FWHM([O III]) and 2.35 σ_* in most Seyferts suggests that the widths of the narrow lines are largely determined by virial motion in the bulge of the host galaxy, although objects with radio jets tend to have systematically broader emission lines for a given σ_*. Interestingly, POX 52 follows this trend almost perfectly, with $2.35\sigma_* = 85 \pm 12$ km s^{-1}, nearly equal to the [O III] FWHM of 87 ± 10 km s^{-1}. This result extends the Nelson & Whittle correlation to Seyfert galaxies with velocity dispersions below 40 km s^{-1}, which may be of use for applying the $M_{\rm BH}$-σ_* relation to other POX 52–like objects whose stellar continua are too faint or too diluted by AGN emission for σ_* to be measured directly. (KSB reached a different conclusion regarding the NLR dynamics, because of their erroneous measurement of the emission-line widths.)

We note that POX 52 is probably not a Wolf-Rayet galaxy, contrary to the conjecture by KSB. In Wolf-Rayet galaxies, the emission bump surrounding 4686 Å is a blend of several features including N III λ4640, [Fe III] λ4658, [Ar IV] λ4711, and [Ar IV] λ4740, in addition to He II (e.g., Kunth & Sargent 1981; Schaerer, Contini, & Kunth 1999). None of these features is present in POX 52. Also, the Wolf-Rayet emission bump from C IV λ5808 does not appear in POX 52. There is no other evidence for recent star formation either from spectral features or from the host galaxy colors or morphology. The broad component to He II λ4686 most likely has its origin in the broad-line region of the AGN, rather than in Wolf-Rayet stars.

POX 52 is not a member of a cluster, but a search of the NED database reveals that it lies close to a known galaxy group. The group USGC S178, with $\langle cz \rangle = 6587$ km s^{-1}, is centered at $\alpha = 12^{\rm h}00^{\rm m}10^{\rm s}.1$, $\delta = -20^\circ 27' 58''$ (Ramella et al. 2002). This group has a velocity dispersion of 243 km s^{-1} for the five galaxies that are known to be members. POX 52 is not listed by Ramella et al. as a group member, but its recession velocity fits within this velocity range, and its projected distance from the group center is 1.3 Mpc, so it may be associated with the group although it is well outside the group's central region. The local environment does not, however, yield any clues as to why this particular dwarf galaxy should be undergoing an AGN accretion episode.

6. CONCLUSIONS

New spectra confirm that POX 52 is a genuine Seyfert galaxy, and the broad components seen on the permitted line profiles (first detected by KSB) demonstrate that POX 52 should be classified as a Seyfert 1. The host galaxy morphology is most similar to that of a dwarf elliptical. This is only the second known example of a Seyfert nucleus in a dwarf galaxy, and the first in a dwarf elliptical. The black hole mass, estimated from the Hβ line width–luminosity–mass correlations for Seyferts, is $1.6 \times 10^5\ M_\odot$, and for this value of $M_{\rm BH}$ POX 52 falls very close to the extrapolated $M_{\rm BH}$-σ_* relation of nearby galaxies. If this black hole mass estimate is accurate, then the AGN in POX 52 is likely to be radiating at nearly its maximal rate, with $L_{\rm bol} \sim (0.5-1) \times L_{\rm Edd}$.

With only two known AGNs in dwarf galaxies, little can be said about the statistics or demographics of this class of objects. The small sample can be at least partly attributed to the fact that no systematic searches for AGNs in dwarf galaxies have been carried out. Additional examples could potentially be detected in objective-prism surveys for emission-line galaxies such as the KISS survey (Salzer et al. 2000). Currently, the Sloan Digital Sky Survey presents perhaps the best opportunity to find more members of this apparently rare class of AGNs. A search of the Sloan data archives to select additional Seyfert nuclei in dwarf galaxy hosts is currently underway (Greene & Ho 2004), as a first step toward filling out the census of massive black holes with $M < 10^6\ M_\odot$.

We thank George Becker for assisting with the Keck observations, and Marla Geha and Gary Ferland for helpful discussions. Research by A. J. B. is supported by NASA through Hubble Fellowship grant HST-HF-01134.01-A awarded by STScI, which is operated by AURA, Inc., for NASA, under contract NAS 5-26555. W. L. W. S. acknowledges support from NSF grant AST-0206067. This research has made use of the NASA/IPAC Extragalactic Database (NED), which is operated by the Jet Propulsion Laboratory, California Institute of Technology, under contract with the National Aeronautics and Space Administration. This research has also made use of data obtained from the High Energy Astrophysics Science Archive Research Center (HEASARC), provided by NASA's Goddard Space Flight Center. Some data presented herein were obtained at the W. M. Keck Observatory, which is operated as a scientific partnership among Caltech, the University of California, and NASA. The Observatory was made possible by the generous financial support of the W. M. Keck Foundation. The authors wish to recognize and acknowledge the very significant cultural role and reverence that the summit of Mauna Kea has always had within the indigenous Hawaiian community. We are most fortunate to have the opportunity to conduct observations from this mountain.

REFERENCES

Barth, A. J. 2004, in Carnegie Obs. Astrophys. Ser. Vol. 1, Coevolution of Black Holes and Galaxies, ed. L. C. Ho (Cambridge: Cambridge Univ. Press), in press (astro-ph/0310436)
Barth, A. J., Ho, L. C., & Sargent, W. L. W. 2002, AJ, 124, 2607
Bender, R., Burstein, D., & Faber, S. M. 1992, ApJ, 399, 462
Bender, R., Paquet, A., & Nieto, J.-L. 1991, A&A, 246, 349
Boese, F. G. 2000, A&AS, 141, 507
Burstein, D., Bender, R., Faber, S., & Nolthenius, R. 1997, AJ, 114, 1365
Burstein, D., & Heiles, C. 1982, AJ, 87, 1165
Cardelli, J. A., Clayton, G. C., & Mathis, J. S. 1989, ApJ, 345, 245
Condon, J. J., Cotton, W. D., Greisen, E. W., Yin, Q. F., Perley, R. A., Taylor, G. B., & Broderick, J. J. 1998, AJ, 115, 1693
de Vaucouleurs, G. 1948, Ann. d'Astrophys., 11, 247
Dressler, A. 1984, ApJ, 286, 97
Elvis, M., et al. 1994, ApJS, 95, 1
Ferrarese, L., & Merritt, D. 2000, ApJ, 539, L9
Filippenko, A. V., & Ho, L. C. 2003, ApJ, 588, L13
Filippenko, A. V., Ho, L. C., & Sargent, W. L. W. 1993, ApJ, 410, L75
Filippenko, A. V., & Sargent, W. L. W. 1989, ApJ, 342, L11
Gavazzi, G., Zibetti, S., Boselli, A., Franzetti, P., Scodeggio, M., & Martocchi, S. 2001, A&A, 372, 29
Gebhardt, K., et al. 2000, ApJ, 539, L13
Geha, M., Guhathakurta, P., & van der Marel, R. P. 2003, AJ, 126, 1794
Gehrels, N. 1986, ApJ, 303, 336
George, I. M., et al. 2001, ApJ, 559, 167
Greene, J., & Ho, L. C. 2004, ApJ, submitted
Ho, L. C., Filippenko, A. V., & Sargent, W. L. W. 1997, ApJS, 112, 315
Hughes, S. A., Márka, S., Bender, P. L., & Hogan, C. J. 2001, in Proc. APS/DPF/DPB Summer Study on the Future of Particle Physics (Snowmass 2001), ed. N. Graf (eConf C010630) (College Park: Am. Phys. Soc.), 402 (astro-ph/0110349)
Iwasawa, K., Fabian, A. C., Almaini, O., Lira, P., Lawrence, A., Hayashida, K., & Inoue, H. 2000, MNRAS, 318, 879
Kaspi, S., Smith, P. S., Netzer, H., Maoz, D., Jannuzi, B. T., & Giveon, U. 2000, ApJ, 533, 631
Kormendy, J. 2004, in Carnegie Obs. Astrophys. Ser. Vol. 1, Coevolution of Black Holes and Galaxies, ed. L. C. Ho (Cambridge: Cambridge Univ. Press), in press (astro-ph/0306353)
Kormendy, J., & Gebhardt, K. 2001, in 20th Texas Symp. on Relativistic Astrophysics, ed. J. C. Wheeler & H. Martel (New York: AIP), 363
Kraemer, S. B., Ho, L. C., Crenshaw, D. M., Shields, J. C., & Filippenko, A. V. 1999, ApJ, 520, 564
Kunth, D., & Sargent, W. L. W. 1981, A&A, 101, L5
Kunth, D., Sargent, W. L. W., & Bothun, G. D. 1987, AJ, 93, 29 (KSB)
Kunth, D., Sargent, W. L. W., & Kowal, C. 1981, A&AS, 44, 229
Landolt, A. U. 1992, AJ, 104, 340
Marconi, A., & Hunt, L. K. 2003, ApJ, 589, L21
Moran, E. C., Eracleous, M., Leighly, K. M., Chartas, G., Filippenko, A. V., Ho, L. C., & Blanco, P. R. 2004, ApJ, submitted
Moran, E. C., Filippenko, A. V., Ho, L. C., Shields, J. C., Belloni, T., Comastri, A., Snowden, S. L., & Sramek, R. A. 1999, PASP, 111, 801
Nelson, C. H., & Whittle, M. 1996, ApJ, 465, 96
Osterbrock, D. E. 1981, ApJ, 249, 462
Osterbrock, D. E., & Fulbright, J. P. 1996, PASP, 108, 183
Osterbrock, D. E., & Pogge, R. W. 1985, ApJ, 297, 166
Osterbrock, D. E., Shaw, R. A., & Veilleux, S. 1990, ApJ, 352, 561
Peng, C. Y., Ho, L. C., Impey, C. D., & Rix, H.-W. 2002, AJ, 124, 266
Persson, S. E. 1988, ApJ, 330, 751
Peterson, B. M. 2003, in Active Galactic Nuclei: From Central Engine to Host Galaxy, ed. S. Collin, F. Combes, & I. Shlosman (San Francisco: ASP), 43
Ramella, M., Geller, M. J., Pisani, A., & da Costa, L. N. 2002, AJ, 123, 2976
Salzer, J. J., et al. 2000, AJ, 120, 80
Schaerer, D., Contini, T., & Kunth, D. 1999, A&A, 341, 399
Schlegel, D. J., Finkbeiner, D. P., & Davis, M. 1998, ApJ, 500, 525
Sérsic, J. L. 1968, Atlas de Galaxias Australes (Córdoba: Obs. Astron., Univ. Nac. Córdoba)
Sheinis, A. I., Bolte, M., Epps, H. W., Kibrick, R. I., Miller, J. S., Radovan, M. V., Bigelow, B. C., & Sutin, B. M. 2002, PASP, 114, 851
Shih, D. C., Iwasawa, K., & Fabian, A. C. 2003, MNRAS, 341, 973
Simien, F., & Prugniel, P. 1998, A&AS, 131, 287
Tremaine, S., et al. 2002, ApJ, 574, 740
van der Marel, R. P. 2004, in Carnegie Obs. Astrophys. Ser. Vol. 1, Coevolution of Black Holes and Galaxies, ed. L. C. Ho (Cambridge: Cambridge Univ. Press), in press (astro-ph/0302101)
Vestergaard, M. 2002, ApJ, 571, 733
Voges, W., et al. 1999, A&A, 349, 389
Whittle, M. 1992, ApJS, 79, 49
Wrobel, J. M., Fassnacht, C. D., & Ho, L. C. 2001, ApJ, 553, L23